Journal Pre-proof

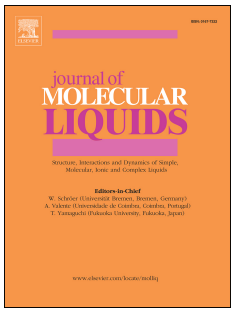

Isoxazoline- and isoxazole-liquid crystalline schiff bases: A puzzling game dictated by entropy and enthalpy effects

Luma Fritsch, Luis A. Baptista, Ivan H. Bechtold, Guilherme Araújo, Richard J. Mandle, Aloir A. Merlo

PII: S0167-7322(19)33369-0

DOI: https://doi.org/10.1016/j.molliq.2019.111750

Reference: MOLLIQ 111750

To appear in: *Journal of Molecular Liquids*

Received Date: 14 June 2019

Revised Date: 12 September 2019

Accepted Date: 14 September 2019

Please cite this article as: L. Fritsch, L.A. Baptista, I.H. Bechtold, G. Araújo, R.J. Mandle, A.A. Merlo, Isoxazoline- and isoxazole-liquid crystalline schiff bases: A puzzling game dictated by entropy and enthalpy effects, *Journal of Molecular Liquids* (2019), doi: https://doi.org/10.1016/j.molliq.2019.111750.

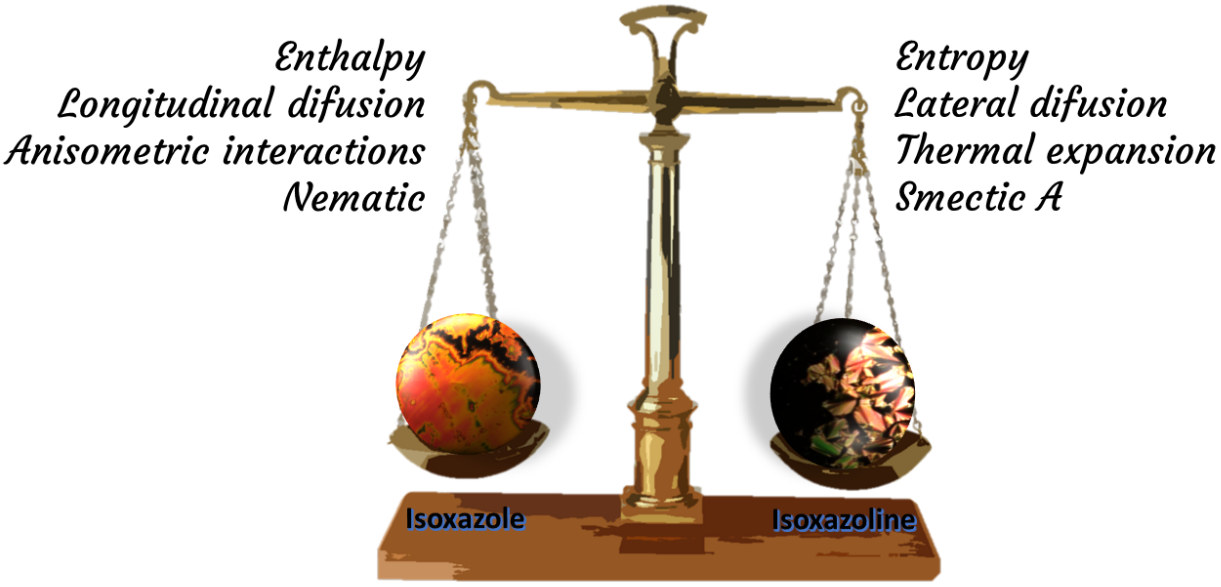
Enthalpy
Longitudinal difusion
Anisometric interactions
Nematic
Entropy
Lateral difusion
Thermal expansion
Smectic A
Isoxazole
Isoxazoline

Isoxazoline- and Isoxazole-liquid crystalline Schiff bases: A puzzling game dictated by entropy and enthalpy effects

Luma Fritsch,[1] Luis A. Baptista,[1] Ivan H. Bechtold,[2] Guilherme Araújo,[1] Richard J. Mandle,[3] and Aloir A. Merlo[1*]

[1]Instituto de Química, Universidade Federal do Rio Grande do Sul, 91501-970, Porto Alegre, RS, Brazil

[2]Departamento de Física, Universidade Federal de Santa Catarina, 88040-900, Florianópolis, SC, Brazil

[3]Department of Chemistry, University of York, York, UK

Corresponding author email: aloir.merlo@ufrgs.br

Abstract

Two series of Schiff base (SB) liquid crystals (LC) containing the 5-membered rings isoxazoline or isoxazole were synthesized and characterized; 27 isoxazoline and 20 isoxazole compounds were obtained. Nematic, smectic A, and smectic C mesophases were found and characterized by Polarized optical microscopy (POM), Differential scanning calorimetry (DSC), and X-ray diffraction. The scientific problem addressed was how the isoxazoline and isoxazole rings affect the mesophase structure and stability. Molecular packing and anisotropic interactions based on enthalpy and entropy properties were used to explain the thermal and structural behaviour observed for both series. The proposed mechanism was assisted by Density functional theory (DFT) calculations, providing new insights into the molecular organization of this kind of system.

Keywords: Liquid crystals; isoxazolines; isoxazoles; entropy effects; enthalpy effects.

1. Introduction

Isoxazolines and isoxazoles have proven to be privileged structures in pharmaceutical and biological areas.[1–10] As an example of a privileged natural structure, acivicin, an isoxazoline derivative, was the inspiration for the synthesis of a collection of new molecular probes for bacterial proteome analysis.[11] Considering their similar molecular connectivities with isoxazolines, isoxazoles are also found in many pharmaceutical applications, and they have been classified as privileged structures. As an example, nonsteroidal anti-inflammatory drugs (NSAIDs) are widely used for the treatment of pain and inflammation, especially

arthritis. NSAID drugs act as aspirin, whose function is to block the formation of prostaglandins (PGs) originating from arachidonic acid by the cyclooxygenase (COX) enzyme. Valdecoxib is one isoxazole example that has been tested as a potent and selective inhibitor of COX-2.[12] The combination of two or more pharmacophore groups in a single molecule enhances biological activity. In this regard, isoxazolines linked tetrazoles and uracils tethered to isoxazoles, isoxazolines and triazoles were prepared for biological screening.[13,14]

The concept of privileged structures can be transferred to functional materials, where some structural, electronic, and morphological prerequisites are required. In liquid crystal science, it is well-established that mesomorphic properties represent a delicate balance between steric constrains and anisotropic attractive interaction.[15–23]

According to the best expert in thermotropic liquid crystal behaviour, visual inspection of the molecular framework drawn on a piece of paper is almost decisive to define if such a virtual molecule could be a liquid crystal (LC). Visual inspection works very well in almost all situations. The decision is guided by some general rules established a long time ago based on structural and electronic prerequisites that molecules need to have.[24]

Rod-shaped molecules tend to be ordinary liquid crystals (calamitic liquid crystals, CLCs), and disc-shaped molecules may present columnar LC behaviour. On the other hand, bent-shaped molecules favour the appearance of an unusual polar order, or, as chameleons, some conformational issues can induce two distinct liquid crystal behaviours and make it difficult to define the existence of mesomorphism and the kind of mesophase.[25] In this context, isoxazolines and isoxazoles open new perspectives in organic synthesis to be explored by the organic experimentalist. In fact, they have been explored by us and others[26–34] in the synthesis and characterization of new liquid crystal compounds. As expected, isoxazolines and isoxazoles usually act as CLCs[35] and, more recently, as banana liquid crystals.[36] Our progress in the preparation of LCs based on isoxazolines, isoxazoles, thiazoline, and thiazoles has shown that they can also produce a false impression as to their identity as a LC. This is especially the case for molecules with a match and mismatch of hydrogenated and perfluorated alkyl chains.[36–38] Five-membered aromatic heterocycles represent an interesting class of organic compounds to be explored in LCs due to their ability to perform very well as mesogenic inductors. Less usual in LCs is the use of non-aromatic 5-membered heterocyclic compounds. Facing the issues related to the existence of a mesophase in 5-membered 3,5-disubstituted isoxazolines, we present our findings regarding the LC behaviour of two series of Schiff bases (SBs) containing isoxazoline (**9**) and isoxazole (**10**) rings (Figure 1). The SB **9** series carries a non-planar 5-membered heterocyclic isoxazoline, while the SB **10** series carries a planar and aromatic 5-membered heterocyclic isoxazole. The carbon atom, indicated by the arrow, defines the mesophase window, thermal stability of the crystal phase, and the mesophase. Relevant to this subject is the relationship between the enthalpy and entropy of these two series of SBs. A puzzling game was established with those energetic parameters. They were tentatively used to explain the mesomorphic behaviour of the **9** and **10** series in terms of steric demands and anisotropic interactions in the mesophase and in the solid state.

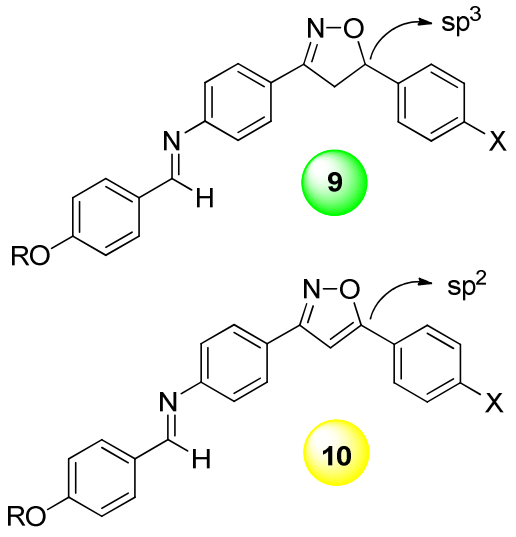

Figure 1. Molecular structure of Schiff bases (SBs) containing isoxazoline **9** and isoxazole **10** rings.

2. Results and discussion

2.1. Synthetic procedures

Our target molecules, SBs **9** and **10**, were synthesized by two molecular partnerships: anilines **6** and **7** and aldehydes **8**. To perform as LCs, heterocyclic rings were installed on the aniline component. In this way, isoxazolines and isoxazoles were chosen, considering our previous results concerning the properties of LCs.[39,40] Isoxazoles can be derived in two steps: by oxidation from isoxazolines,[41] which were in turn built up via [3+2] 1,3-dipolar cycloaddition between oxime **2** and styrenes **3**.[42]

Scheme 1 and Scheme 2 describe our strategy to build the heterocyclic isoxazolines and isoxazoles in a straightforward way. Aldehyde **1** and styrenes **3a–f** are commercially available chemicals. Oximation of **1** yielded *p*-nitrobenzaldehyde oxime **2,** which precipitated at the end of the reaction when the temperature dropped to room temperature. It was collected as a crystalline solid, without the need for recrystallization. Next, oxime **2** was exposed to a 5% aqueous solution of $NaOCl/CH_2Cl_2$ to give, *in situ*, the reactive nitrile oxide, which was captured by styrenes **3a–f**. The cycloadducts **4a–f** were obtained in fair to good yields. Oxidation of the isoxazoline ring was performed using γ-MnO_2 under toluene refluxing, producing isoxazoles **5a–d** and **5f**. Transformations of **4a–f** to **5a–f** convert less anisotropic isoxazolines to more anisotropic isoxazoles or *pre-mesogenic* ones.[16] Compounds **4e**,**4f** and **5f** are useful intermediates to be used in more elongated and anisotropic molecules. Acetyl and *tert*-butyl protecting groups can be removed, providing the respective phenols **4g** and **5g**.

In doing so, removal of the protecting groups followed by Williamson alkylation with linear and branched alkyl bromides, such as *n*-butyl bromide and 2-ethylhexyl bromide, gave **4h–i** and **5h–i** in good yields.

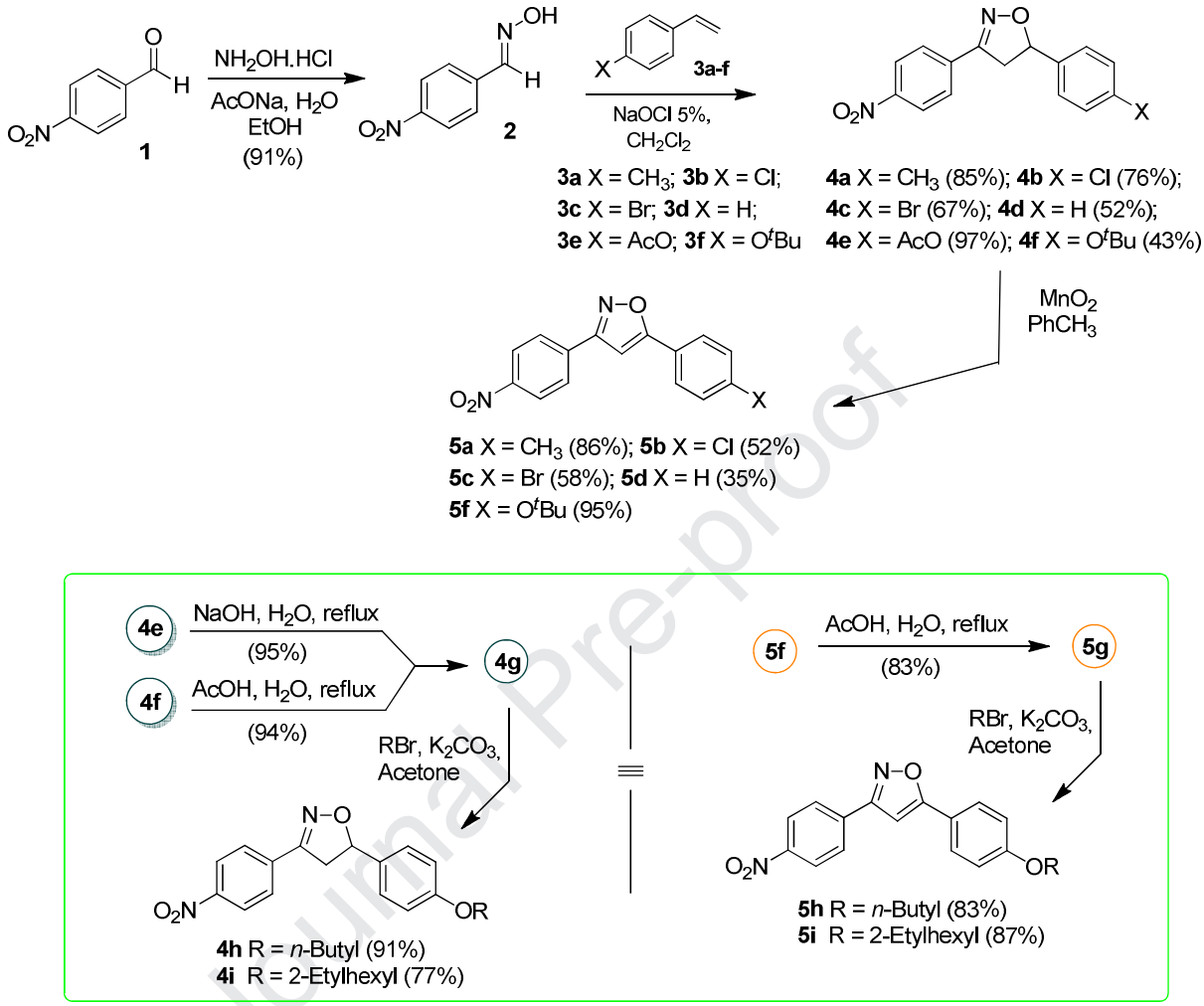

Scheme 1. Synthesis of isoxazolines **5a–f** precursors and **4h–i** and **5h–i** intermediates.

The next step in our strategy was to prepare a collection of anilines **6a–f** and anilines **7a–f**. Reduction of the nitro group to the aniline group was done using $SnCl_2.2H_2O$ as the reducing agent. The reaction was conducted under a nitrogen atmosphere and with absolute ethanol as a solvent, as outlined in Scheme 2. The yields of the amino isoxazoles containing an alkyl group were fair to low in general. We adopted this methodology because the traditional reaction using H_2 and Pd/C had failed, especially with isoxazoline derivatives. The heterocyclic reduction to 1,3-aminoalcoohol was the main collateral reaction observed.

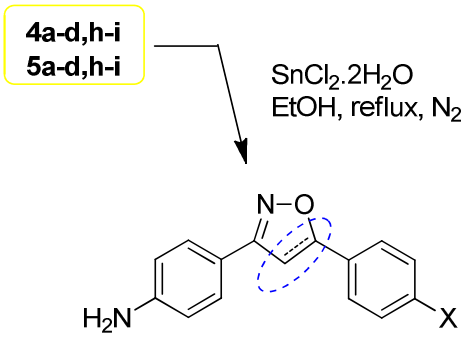

Isoxazolines	Isoxazoles
6a X = CH_3 (89%)	**7a** X = CH_3 (64%)
6b X = Cl (92%)	**7b** X = Cl (91%)
6c X = Br (70%)	**7c** X = Br (91%)
6d X = H (86%)	**7d** X = H (46%)
6e X = OC_4H_9 (91%)	**7e** X = OC_4H_9 (35%)
6f X = O-2-Ethylhexyl (32%)	**7f** X = O-2-Ethylhexyl (43%)

Scheme 2. Reduction reaction of nitro compounds to anilines **6a–f** and **7a–d**.

Scheme 3 outlines the Schiff bases **9a*n*–9f*n*** and **10a*n*–10f*n***. The condensation reaction between anilines **6a–f** and **7a–f** and aldehydes **8a–d** with acetic acid was done in ethanol under reflux for 2 h. At the end, the solution was cooled and the products were collected as a precipitated solid. SBs were isolated as a solid powder. Purification was done by two or three recrystallizations in ethanol. Solids obtained were resolubilized in DCM, and SB solutions were filtrated using Millipore filters. A collection of 27 isoxazolines and 20 isoxazoles was prepared. The descriptor *n* in the code indicates the number of carbon atoms that belong to the linear alkyl chain bonded in aromatic aldehydes.

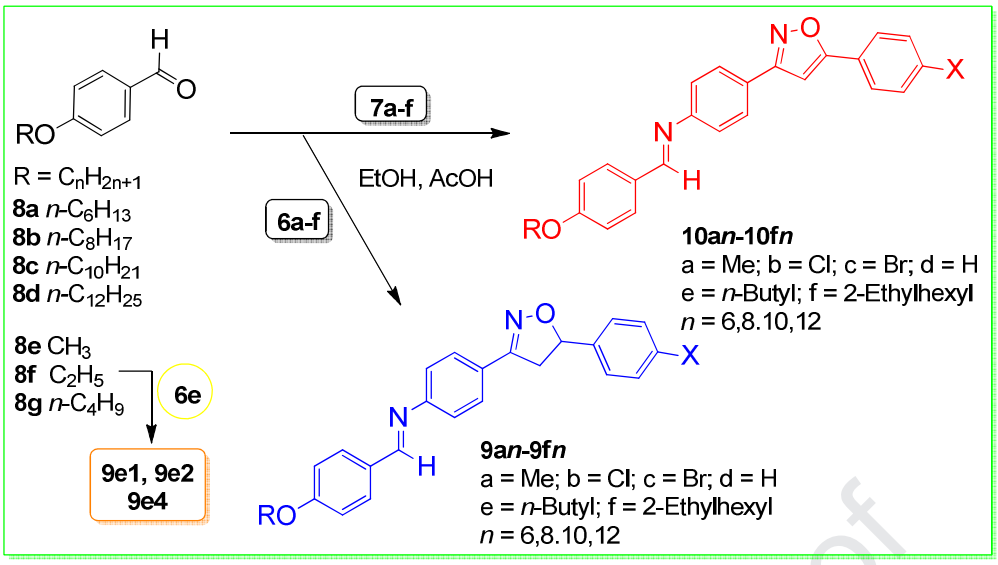

Scheme 3. Preparation of SBs **9a*n*–9f*n*** and **10a*n*–10f*n***.

All final LC compounds were characterized by ^{1}H and ^{13}C NMR spectral and thermal analysis (DSC and POM). Experimental descriptions, as well DSC traces and ^{1}H and ^{13}C NMR spectroscopic characterizations, are available in the supporting information (SI).

2.2. Liquid-Crystalline Properties

All final compounds showed mesomorphic behaviour, considering that molecules in these series have rod-shape topologies. The transitional properties for all molecules with isoxazoline and isoxazoles nuclei are given in Table 1 and Table 2, respectively. For both series, 6 sets of liquid crystals were prepared for each series, **9an–9fn** and **10an–10fn**, with *n* representing the linear alkyl chain (n=1, 2, 4, 6, 8, 10, and 12 carbon atoms) in one terminus of the rigid core, while the other terminus contains a substituent X that differs in shape and polar nature (a = Me, methyl; b = Cl, chlorine; c = Br, bromine; d = H, hydrogen; e = But, *n*-butyl; and f = 2-EtHex, 2-ethylhexyl).

Figures 2–4 display some pictures that were selected for series **9** and **10** and were taken by POM. Figure 2a displays the SmA texture of compound **9b8** with a polar chlorine group, which was identified by the focal conic domains (FCDs) for the sample covered by a cover glass and the parabolic (polygonal) texture outside the cover glass. Figure 2b displays the texture of the nematic mesophase for **9d6**, with black and coloured areas being relative to the homeotropic and planar texture, respectively. Upon cooling, the transition between the isotropic liquid phase and the N mesophase is seen by nematic droplets that formed at the bottom left corner of Figure 2b. Figure 2c shows two distinct areas of SmC texture obtained upon cooling at 150°C of **9e8**. Broken focal-conic fan-shaped defects combined with flash and bright areas of the Schlieren texture of SmC are seen for **9e8**. Figure 2d displays Schlieren texture with typical gray disclination points and lines of **9e12**. Compounds with short alkyl chains, such as **9e1** (methyl), **9e2** (ethyl), and **9e4** (*n*-butyl), showed the N

mesophase, while **9e6**–**9e12**, containing medium and long alkyl chains, presented the SmC mesophase. Two examples of Schlieren texture of the SmC mesophase can be seen in Figure 2c,d. The nematic mesophase was observed for compounds without substituent at the para-position of the phenyl ring (**9d6** and **9d8**).

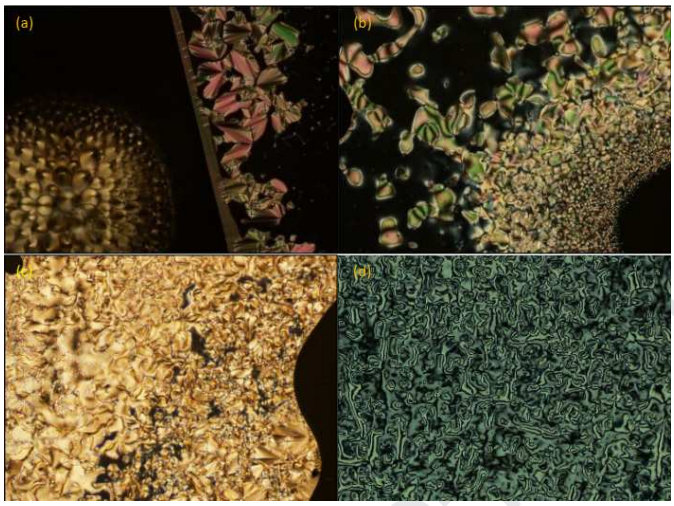

Figure 2. (a) Focal conic defects and homeotropic texture in the SmA mesophase for **9b8** upon cooling at 184°C (2nd heating scan). Polygonal texture at left side without coverslip and focal conic domains at right side. (b) Schlieren and homeotropic texture for monotropic N mesophase for **9d6**. (c) SmC mesophase for **9e8** upon cooling at 150°C. (d) Schlieren texture of the SmC mesophase for **9e12**.

Table 1. Phase transition temperatures for isoxazolines Schiff bases **9**.

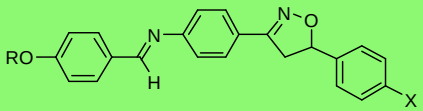

Entry	R	X	Transition Temperatures (°C)[a] [Enthalpy (kJ.mol^{-1})] {Entropy (J.mol^{-1}K^{-1})}								
			Cr		SmC		SmA		N		I
9a6	C_6H_{13}	Me	●	144[37.5]{89.9}[b,c]	-	-	●	(135)	●	159 [0.35]{0.80}	●
9a8	C_8H_{17}	Me	●	140 [25.0]{61.3}[b,d]	-	-	●	149 [0.92]{2.20}	●	155 [0.57]{1.32}	●
9a10	$C_{10}H_{21}$	Me	●	138 [25.6]{63.4}[b,d]	-	-	●	155 [5.04]{11.6}	-	-	●
9a12	$C_{12}H_{25}$	Me	●	135 [34.8]{85.5}[b]	-	-	●	154 [6.60]{15.4}	-	-	●
9b6	C_6H_{13}	Cl	●	159 [24.7]{57.1}	-	-	●	183 [4.70]{10.3}	-	-	●
9b8	C_8H_{17}	Cl	●	149 [49.5]{117}	-	-	●	183 [12.7]{27.8}	-	-	●
9b10	$C_{10}H_{21}$	Cl	●	141 [32.8]{79.2}[c]	-	-	●	183 [8.50]{18.6}	-	-	●
9b12	$C_{12}H_{25}$	Cl	●	134 [29.7]{73.1}	-	-	●	179 [4.56]{10.1}	-	-	●
9c6	C_6H_{13}	Br	●	169 [44.0]{99.6}	-	-	●	184 [7.30]{15.9}	-	-	●
9c8	C_8H_{17}	Br	●	161 [36.4]{83.8}[b]	-	-	●	186 [8.50]{18.5}	-	-	●
9c10	$C_{10}H_{21}$	Br	●	152 [28.5]{67.1}	-	-	●	184 [7.22]{15.8}	-	-	●
9c12	$C_{12}H_{25}$	Br	●	148 [28.1]{66.6}	-	-	●	182 [7.36]{16.2}	-	-	●
9d6	C_6H_{13}	H	●	139 [38.4]{93.1}	-	-	●	(128) [1.14]{2.83}	●	(140)[e] [0.71]{1.73}	●
9d8	C_8H_{17}	H	●	139 [46.8]{113}	-	-	●	(128) [0.98]{2.45}	●	(141)[e] [4.32]{10.5}	●
9d10	$C_{10}H_{21}$	H	●	137 [38.7]{94.3}	-	-	●	144 [5.31]{12.7}	-	-	●
9d12	$C_{12}H_{25}$	H	●	136 [36.3]{88.7}	-	-	●	147 [5.67]{13.5}	-	-	●
9e1	CH_3	*n*-BuO	●	153 [29.0]{68.0}	-	-	-	-	●	166 [0.36]{0.83}	●
9e2	C_2H_5	*n*-BuO	●	148 [22.5]{54.0}	-	-	-	-	●	177 [0.42]{0.92}	●
9e4	C_4H_9	*n*-BuO	●	156[31.2]{73.0}	-	-	-	-	●	170 [0.63]{1.50}	●
9e6	C_6H_{13}	*n*-BuO	●	148 [25.1]{59.6}[f]	●	149 [0.16]{0.39}	●	162 [0.19]{0.43}	●	169 [1.38]{3.11}	●
9e8	C_8H_{17}	*n*-BuO	●	138 [24.8]{60.5}[b]	●	158 [3.60]{8.30}	-	-	-	-	●
9e10	$C_{10}H_{21}$	*n*-BuO	●	134 [24.3]{59.8}	●	161 [5.90]{13.6}	-	-	-	-	●
9e12	$C_{12}H_{25}$	*n*-BuO	●	133 [30.9]{76.3}	●	162 [7.31]{16.8}	-	-	-	-	●
9f6	C_6H_{13}	2-EtHexO	●	86 [13.2]{36.8}[f]	●	116[0.12]{0.31}	●	124 [3.20]{8.06}	-	-	●
9f8	C_8H_{17}	2-EtHexO	●	93 [15.4]{42.1}[c]	●	115 [2.30]{5.87}	-	-	-	-	●
9f10	$C_{10}H_{21}$	2-EtHexO	●	93 [20.7]{56.7}	●	124 [6.31]{15.9}	-	-	-	-	●
9f12	$C_{12}H_{25}$	2-EtHexO	●	97 [21.4]{57.7}	●	122 [6.10]{15.4}	-	-	-	-	●

Scan rate = 10°C min^{-1} for all samples. Cr denotes the crystal phase. SmC = Smectic C phase, SmA = Smectic A phase, and N = Nematic phase. Monotropic N, SmA, and SmC mesophases observed by POM upon cooling are in parentheses. The transition temperatures and enthalpy values were collected from a second heating scan to the isoxazolines-BS. [a]Tonset was considered for crystal to mesophase only. [b]Reference 39. [c]Reference 40. [d]Values for enthalpy and entropy for the transition between crystal phases were summed. [e]Peak temperature. [f]Scan rate = 2°C min^{-1} .

Table 2. Phase transition temperatures for isoxazoles Schiff bases **10**.

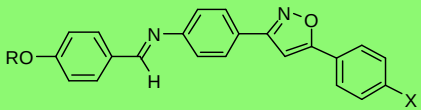

Entry	R	X	Transition Temperatures (°C) [Enthalpy (kJ.mol^{-1})] {Entropy (J.mol^{-1}K^{-1})}								
			Cr		SmC		SmA		N		I
10a6	C_6H_{13}	Me	●	143 [32.3]{77.6}[b,c]	-	-	-	-	●	287 [0.48]{0.85}	●
10a8	C_8H_{17}	Me	●	141 [37.3]{90,0}[b]	-	-	-	-	●	278 [0.68]{1.24}	●
10a10	$C_{10}H_{21}$	Me	●	125 [23.1]{58.1}[b]	●	(140)	-	-	●	253 [0.44]{0.84}	●
10a12	$C_{12}H_{25}$	Me	●	126 [44.0]{110.1}[b]	●	178 [0.32]{0.70}	-	-	●	255 [1.05]{1.99}	●
10b6	C_6H_{13}	Cl	●	130 [34.8]{86.4}	-	-	●	278 [0.70]{1.26}	●	304 [0.68]{1.17}	●
10b8	C_8H_{17}	Cl	●	128 [39.8]{99.4}	-	-	●	289 [3.07]{5.48}	-	-	●
10b10	$C_{10}H_{21}$	Cl	●	126 [47.7]{119,5}[c]	-	-	●	293 [5.19]{9.18}	-	-	●
10b12	$C_{12}H_{25}$	Cl	●	127 [52.4]{131,1}	-	-	●	288 [5.75]{10.3}	-	-	●
10c6	C_6H_{13}	Br	●	143 [30.9]{74.3}	-	-	●	299 [0.60]{1.03}	●	316 [0.27]{0.46}	●
10c8	C_8H_{17}	Br	●	137 [53.8]{131.4}	-	-	●	301 [5.52]{9.63}	-	-	●
10c10	$C_{10}H_{21}$	Br	●	132 [50.7]{125.2}[b]	-	-	●	295 [4.50]{7.93}	-	-	●
10c12	$C_{12}H_{25}$	Br	●	129 [54.2]{134.6}	-	-	●	280 [4.30]{7.71}	-	-	●
10d6	C_6H_{13}	H	●	135 [39.9]{97.7}	-	-	-	-	●	231 [0.54]{1.06}	●
10d8	C_8H_{17}	H	●	129 [38.7]{98.0}[d]	-	-	-	-	●	224 [0.53]{1.07}	●
10d10	$C_{10}H_{21}$	H	●	139 [33.7]{101.8}[d]	-	-	-	-	●	198 [0.41]{0.90}	●
10d12	$C_{12}H_{25}$	H	●	118 [52.6]{134.7}	-	-	-	-	●	205 [0.59]{1.23}	●
10e6	C_6H_{13}	*n*-BuO	●	118 [17.9]{45.8}	-	-	-	-	●	270 [3.01]{7.54}	●
10e8	C_8H_{17}	*n*-BuO	●	122 [17.0]{43.1}[b]	●	248 [1.09]{2.10}	-	-	-	-	●
10f6	C_6H_{13}	2-EtHexO	●	96 [17.2]{46.7}	●	139 [0.71]{1.72}	-	-	●	173 [0.71]{1.60}	●
10f8	C_8H_{17}	2-EtHexO	●	100 [34.7]{93.2}[c]	●	146 [0.88]{2.10}	-	-	-	-	●

Scan rate = 10°C min^{-1} for all samples. Cr denotes the crystal phase, SmC = Smectic C phase, SmA = Smectic A phase, and N = Nematic phase. Monotropic SmA and SmC mesophases observed by POM upon cooling are in parentheses. The transition temperatures and enthalpy values were collected from the first cycle for the isoxazole-BS. [a]Tonset was for the crystal to mesophase only. [b]Reference 39. [c]Reference 40. [d]Values for enthalpy and entropy for the transition between crystal phases were summed.

Figure 3 displays the texture presenting the undulation phenomenon [43,44] observed for isoxazoline **9e6**. The mesophase sequence Cr 148 SmC 149 SmA 162 N 169 Iso was assigned. Some comments will be addressed to the LC behaviour of **9e6** concerning its nematic mesophase texture in SI section

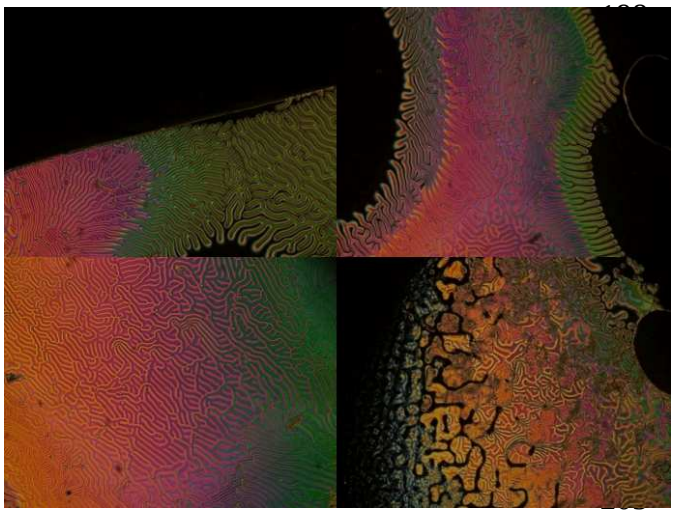

Figure 3. Polarizing optical microscopy (POM) images of the fingerprint texture observed for SB **9e6** as the temperature approaches the transition to the isotropic state.

Figure 4 displays the representative textures for SBs containing the isoxazole ring. Three SBs were selected and the texture was briefly described.[45] A planar texture of the N mesophase is shown in Figure 4a for compound **10d10** near to the transition temperature to the isotropic state. From left to right in Figure 4a, a dark red wave is seen, which flows over the dark yellow region, leaving behind bubbles of air and black areas. Figure 4b shows the SmC mesophase in two distinct defects - a grainy schlieren texture at the left and a broken fan-shaped texture at the right for compound **10e8** at 230°C. A classical Schlieren texture of the nematic mesophase is shown in Figure 4c for compound **10f6**. In Figure 4d, the transition between SmC and N mesophases upon cooling for **10f6** is shown. At the left side, the texture is brighter than the right side due to freedom of the phase director in the N mesophase and the greater order in the smectic mesophase.

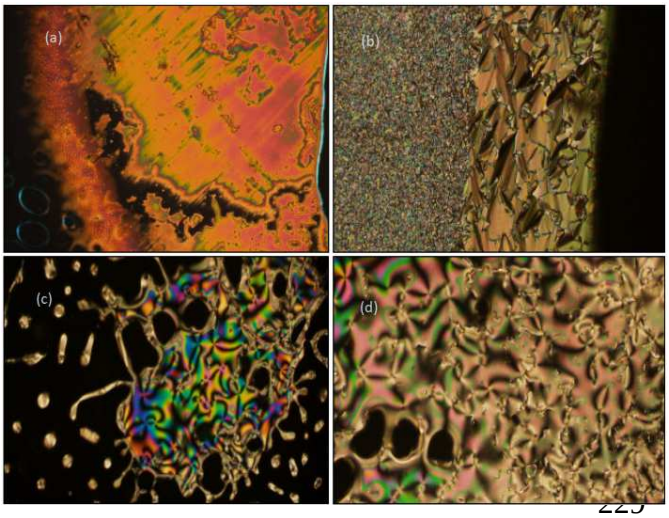

Figure 4. (a) Planar texture for the nematic mesophase of **10d10** upon heating. (b) Grainy Schlieren texture (at left) and broken fan focal conic texture (at right) for SmC upon cooling for **10e8**. (c) Schlieren texture upon heating for **10f6** at 230°C and (d) Schlieren texture for the N → SmC transition upon cooling.

Upon examination of the transitional properties of this series, some trends may be drawn according to data in Table 1. The series containing small and polar terminal groups connected to the phenyl ring at the 5-position of the heterocyclic ring (methyl, chlorine, bromine, and hydrogen) displayed SmA and/or N mesophases. For medium and large alkyl groups in the same phenyl ring (*n*-butyl and 2-ethylhexyl), the tilted SmC and nematic mesophases are predominant. The mesophase range and type for all LC compounds listed in Table 1 and Table 2 are dependent on the nature of the heterocyclic ring. The SmA mesophase was found for compounds **9an**, **9bn**, **9cn**, **9dn**, and **9f6**. However, for series **10** only **10bn** and **10cn** displayed the SmA mesophase. Inversely, the N mesophase was mandatory for series **10**. As a general outcome, the results confirm that isoxazole is by far the best molecular moiety to induce mesomorphism. The isoxazoline ring, even being a non-planar core due to tetrahedral carbon atoms inserted into its framework, is also a mesophase molecular inductor. The ranges of mesophases for isoxazolines were about 20°C. On the other hand, the isoxazole nucleus showed an expressive wide mesophase range, sometimes higher than 150°C. That is a huge mesophase stability, like compound **10b6,** where the range up to 174°C. Anisotropic interactions originating from the planarity and more extensive resonance conjugation are the reasons for the high mesophase stability of the isoxazole ring in the mesophase, allowing it to interact in a more effective manner in the condensed and fluid state through a π-stacking interaction.[29,] The main drawback of SBs containing the isoxazoles in this series is that their thermal decomposition upon heating becomes more intense when the samples are exposed to high temperatures, especially when the temperature ranges of the analyses cross the line of the mesomorphic state to isotropic state. This is the price to pay to be more stable and to resist losing their orientational order when going to the isotropic state due to the efficient intermolecular interaction across the 3,5-diarylisoxazole system. DSC

thermograms in Figure 5 represent this behaviour. Whereas **9c10** displays stable behaviour during the second cycle of heating and cooling in the range of 60–220°C, **10c10** decomposes during the first cycle of heating when the sample is exposed to temperatures of 60–350°C. In general, temperatures of melting for isoxazolines are higher than the isoxazole ring. In contrast, isoxazoles display high values of clearing temperature. Thermal stability here is a relative concept considering that the LC behaviour remains stable for the isoxazoline series due to the low value of the isotropic transition temperature. This means that the thermal stability depends on the mesophase range under observation.

Enthalpy and entropy values are dependent on both the nature of the transition temperature that has been considered and the heterocyclic nuclei present in these SBs. In general, enthalpy and entropy values for isoxazoles were superior for the transition of the crystal phase to the mesophase, and they displayed lower enthalpy and entropy values for the transition from the mesophase to the isotropic state. Steric packing considerations are important to mesophase formation for isoxazolines, and anisotropic attractive interactions rather than electrostatics are decisive for the stability of the mesophase in isoxazole systems.

Considering the transitional data exemplified for SBs **9c10** and **10c10,** we can discuss some interesting features of these two SB molecular architectures. The mesophase range for **9c10** is ΔT = 32°C, while for **10c10** it is ΔT = 163°C, being five times higher owing to the fact that the molecular topology favours molecular packing of isoxazole against the isoxazoline ring in the mesophase. Clearing transition temperatures are also very discrepant between them. While **9c10** goes to the isotropic state at 184°C, **10c10** enters the liquid state only at 295°C. Enthalpy and entropy data collected for these SBs are also interesting, which reflect the nature of molecular packing in the solid and in the mesomorphic state.

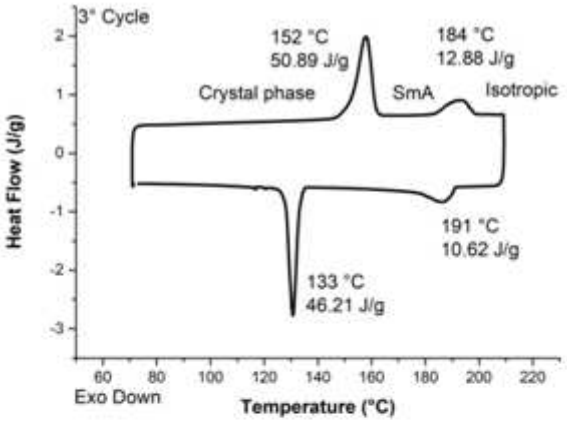

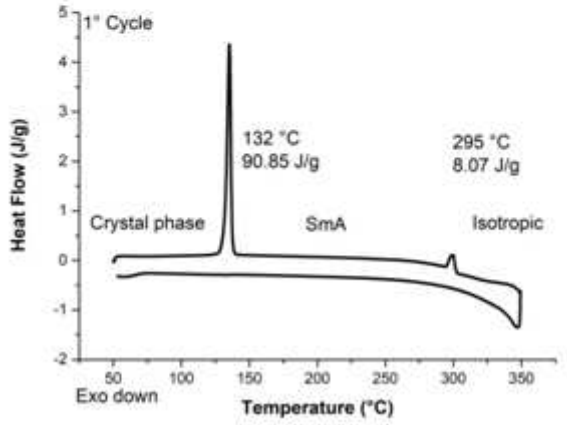

Figure 5. DSC thermogram for compounds **9c10** and **10c10**.

Figure 6 describes the molecular arrangement for SBs **9c10** and **10c10** in the all-*trans* conformation. This helps us to understand more regarding the thermal behaviour and the dependence of the mesophase nature and transition temperatures observed in Table 1 and Table 2. Differences in their LC behaviour cannot be attribute specifically to the electrostatic interactions, considering that both LCs have high and similar dipole values. Estimated values of the dipole moment for **9c10** and **10c10** by DFT calculations are 6.6 D and 5.6 D, respectively.[46] Dipolar moment directions deviate partially from the molecular axis, being more accentuated for isoxazolines **9c10**. Molecular folds for **9c10** and **10c10** are indicated as 132.09° and 155.34°, respectively (SI). The longitudinal and lateral direction given by the dipole moment corroborate the predominance of the nematic mesophase for series **10** and the smectic mesophase for series **9**. Orientational order is gained in series **10**, while positional order is gained in series **9**.

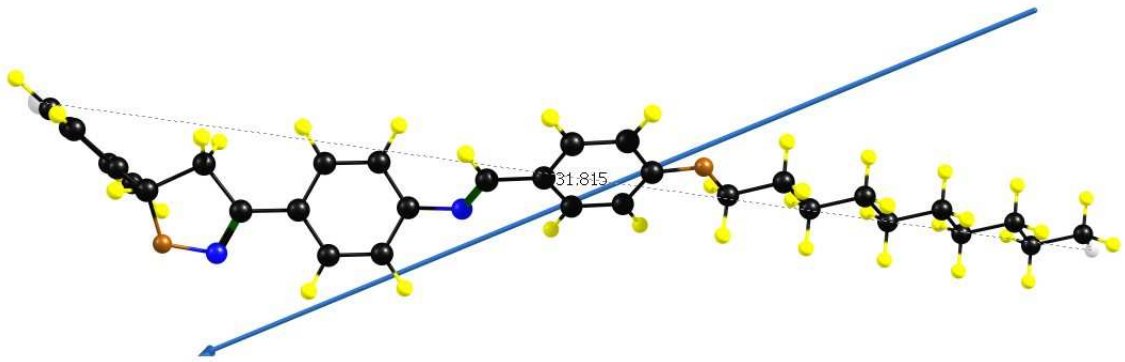

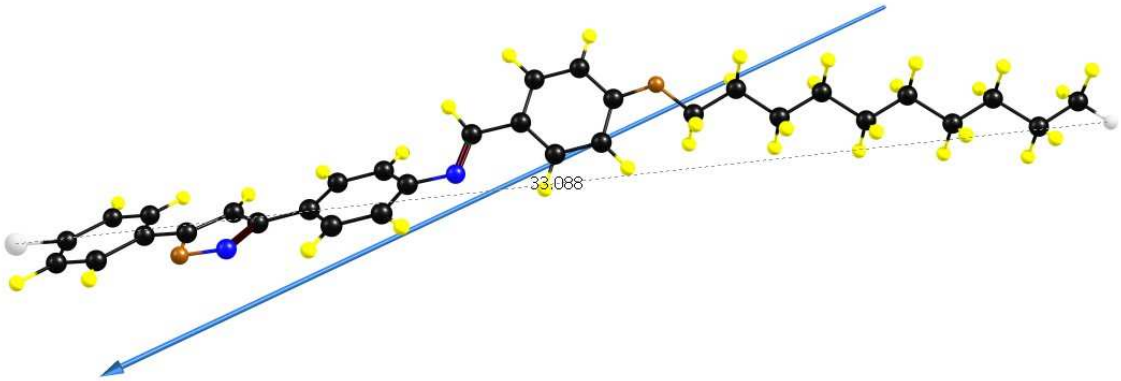

Figure 6. Ball-stick model for compounds **9c10** (up) and **10c10** (down) obtained by molecular modelling and dipolar moments, respectively.

Isoxazolines and isoxazoles can be considered cousin compounds due to their similarity in molecular connectivity. However, despite the same sequence of atoms in their structures, they drastically differ when viewed in three-dimensional (3-D) space. The SBs described in this study assume a hockey-stick shape considering that the length (L_1 and L_2) of the aryl substituent at position 3 and 5 of the heterocyclic compound are not symmetrical in their constitution and are different in length. Estimated DFT values are *ca* 27.3 Å and 6.2 Å for the longest and the shortest aryl groups for **9c10**, respectively. For the isoxazole ring, these two aryl groups are located on the same molecular plane σ (left side of Figure 7) and the angle β describes the molecular bend of the 3,5-disubstituted arylisoxazoles. By changing from isoxazole to isoxazoline, the tetrahedral carbon atoms are inserted into positions 4 and 5, which pull the shorter aryl group off the σ plane (basal plane). Now that aryl groups are no longer positioned in the same plane, the coplanarity is not observed anymore. Molecules change their in-plane hockey-stick shape, as seen in the isoxazole, to assume a new out-of-plane hockey-stick shape in the isoxazolines. Two new angles should be assigned - α is the angle related to how the aryl group is compelled to be off the σ–plane and γ is the new molecular bending of the isoxazoline ring. While the 3,5-disubstituted isoxazole ring has just one molecular plane where all atoms are confined, the 3,5-disubstituted isoxazoline has two molecular planes—the main plane (σ) and a secondary plane (σ´) that contains the shorter aryl group.

For isoxazoles, an anticlinic arrangement of molecules is proposed, according to Figure 7. Molecules alter their relative nitrogen and oxygen heteroatom positions in-layers and out-layers. Inside the layers, molecules change the molecular orientation considering that the heterocyclic ring is non symmetric. By passing from layer to layer, the relative orientation of the molecules is also alternated from right to left and vice-versa in an attempt to adjust the dipole moment. The lamellar structure that emerges displays a packing density superior to the isoxazoline counterparts by π-stacking, and the clearing transition temperatures and the mesophase thermal window for isoxazoles assume higher values than the isoxazolines, as seen in Table 1. For comparative purposes, entropy values of **9c10** and **10c10** associated with the

transition from the crystal phase to the SmA mesophase are 67.1 J mol^{-1} and 125.2 J mol^{-1}, respectively. The entropy value observed, which is almost twice as high for **10c10,** is a direct consequence of the intermolecular interactions in the crystal phase for isoxazoles. In general, enthalpy and entropy values for compounds listed in Table 1 and Table 2 follow this tendency.

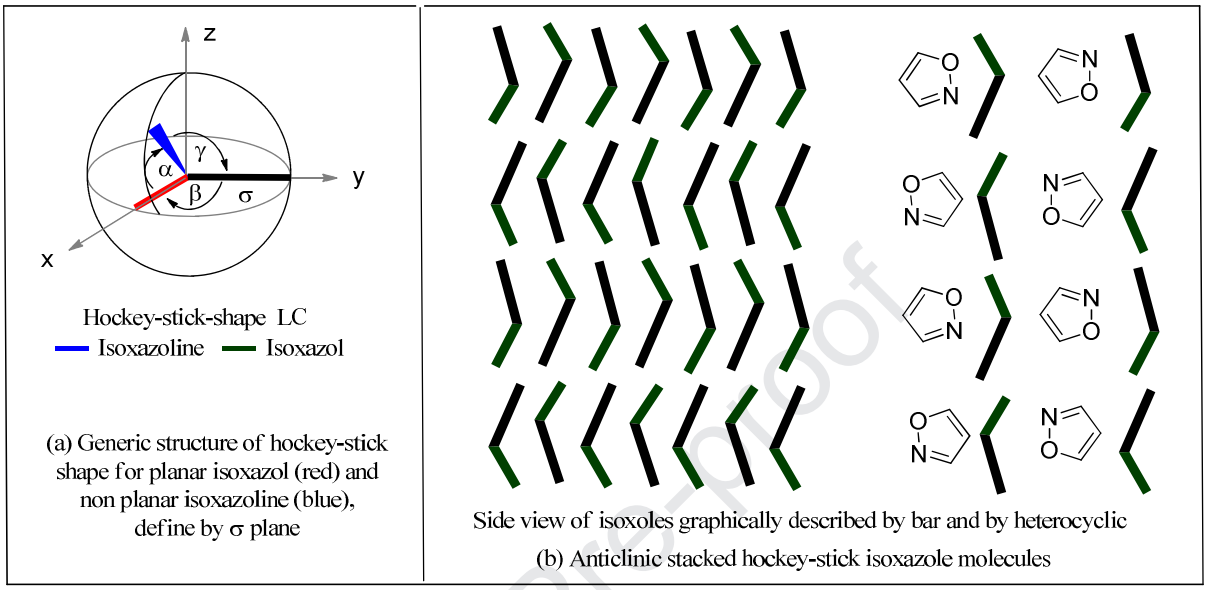

Figure 7. General hockey-stick shape structure and distinct views of the anticlinic arrangements in the SmA mesophase of the hockey-stick shape LC from SBs. From the left side, isoxazoles are represented by a red bar with a bending angle of β and isoxazolines are described by a blue bar with a bending angle of α out of the σ plane – basal plane. The side views describe the hockey-stick molecules in the lamellar structure of the SmA mesophase. At the right, the isoxazole ring orientation is shown as a way to clarify the anticlinic arrangement. The neutrality of the layer is preserved by inversion of the isoxazole ring in-layer and out-layer. In the interlayer, a synclinic molecular disposition is assumed to accommodate interface fluctuations.

A plausible arrangement of isoxazoline compounds is depicted in Figure 8. This is an oversimplified view of the packing manner of the molecules prepared in this work. Attempts to obtain single-crystal resolution of one of the SBs discussed in Table 1 and Table 2 have failed. However, our more recent results have showed that isoxazoles and isoxazolines in their crystal phase are packed in a similar way.[47] The single crystal resolution reported by Zanata[48] and Zerirov[49] also supports our choice, as shown in Figure 8. Figure 8a describes the molecular packing of isoxazoline compounds, considering that it is a racemic mixture and the heterocyclic ring is non symmetrical. Thus, moving laterally from pile to pile, the molecular dipole inverts its direction, pointed in the opposite direction to maintain neutrality of charges between the layers. In layers, molecules develop a lamellar structure on the y-coordinate (in-plane horizontal direction). Considering a racemic mixture, we can envisage four piles of the molecules composed of *R* and *S* enantiomers in a vertical direction

(z-axes). The aromatic moieties in black and blue in Figure 8 are positioned in two distinct molecular planes: the main plane (σ) and a secondary plane (σ´), respectively. This molecular arrangement in the crystal state of the isoxazolines is responsible for lower transitional values than the isoxazoles during the melting process. In Figure 8, the possible molecular arrangements in the crystal phase for isoxazoline based on X-ray data from the literature are shown.[47-49] The chiral centre on the isoxazoline define that the solid could be envisaged being constitute by racemic or homoquiral domains. It does not matter what kind of domain we assume; molecules under these circumstances should retain neutrality in terms of polarity and handness. Figure 8a shows the top view of isoxazoline piles, with their right-handness and left-handness being obey as well as for molecular dipole. Figure 8b is an oversimplified model of the chiral domains in the crystal phase for the (*R*)-isoxazoline configuration. The blue ball and stick drawn in the σ´ plane represent the shortest molecular alkylaryl group connected at the C-5 carbon atom on the isoxazoline ring. The principal molecular plane (σ) contains the longest aryl group connected at the C-3 carbon atom of isoxazoline, and the blue ball up and down represents the chiral centre (*R* or S). In both Figure 7 and Figure 8, anticlinic arrangements are proposed for molecules of the **9** and **10** series. However, in the interface of the layers, if we are independently considering the σ or σ´ plane, the synclinic arrangement is assumed.[50-51] Upon heating, the void volume between σ´ planes increases more significantly than between σ planes (Figure 8d). The compactness in the crystal phase is looser (void volume) for series **9** than series **10**. Conversely, values of the transitional properties (enthalpy and entropy) for the SmA mesophase to the isotropic state are, in general, smaller for isoxazoles than for isoxazolines, as indicated by **9c10** and **10c10** selected for this discussion.

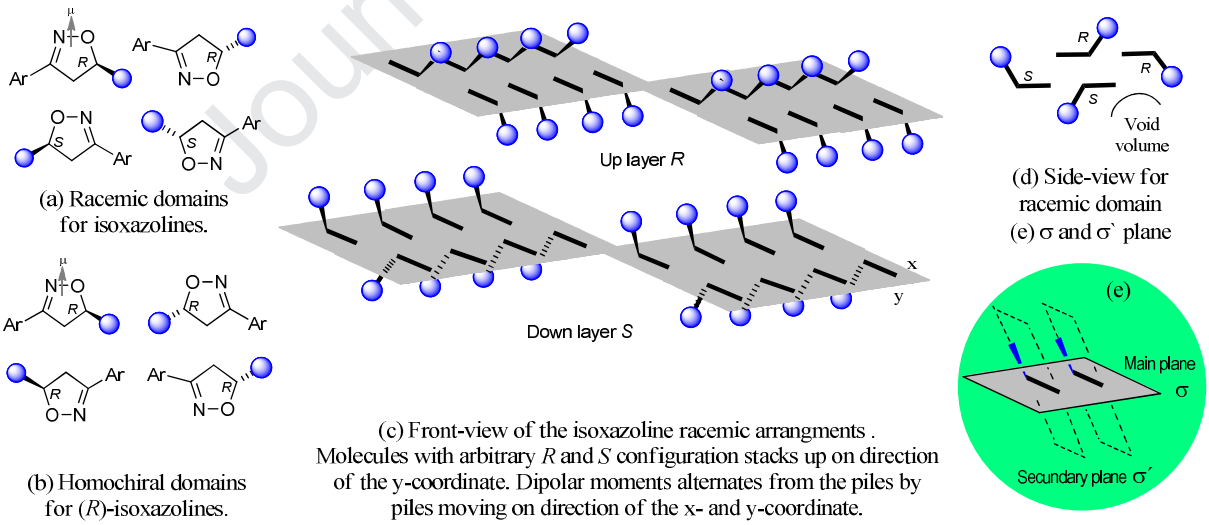

Figure 8. General description of (a) racemic isoxazolines (b) and the homochiral configuration for (*R*)-isoxazolines. (c) Hypothetical molecular arrangement through front- and side-views. Molecules stack up, forming layer structures, and each layer is next to others with the opposite chirality. Each pile has its own handness and its dipole moment is inverted to maintain neutrality. (d) Anticlinic arrangement is reached when a set of four isomers is side-view. (e) Main and secondary plane σ and σ'.

The deviation of linearity as assigned by angles β and γ (Figure 7) of the LCs analysed in this study, as well as the mesomorphic behaviour of series **9** and **10**, are dependent on the type of heterocyclic connecting the two aryl groups at 3- and 5-positions. Data in Table 1 and Table 2 reveals that there is a gain in orientational order for more anisotropic molecules of series **10**, and positional order acts in favour of less linear LCs that belong to series **9**. The molecular bend of non-linear molecules generates geometrical defects on the mesophase structure, which inhibits longitudinal diffusion and imposes a rotational restriction along the phase director. To compensate for the non-linear shape, molecules respond in such a way that they can move laterally, thus favouring the formation of a layered structure by lateral diffusion. Upon cooling, the geometrical constrain of the non-linear molecules becomes more evident and decisive for both the mesophase window and mainly the mesophase nature. The molecular order that increases upon cooling highlights the conflict between molecular packing and steric constraints - the excluded volume manifests itself through the geometric defect. The maximization of available space and, therefore, the minimization of free volume are critical for the formation of nematic or smectic mesophases. Considering that the bending of series **9** is composed of two molecular planes (σ and σ´), while series **10** presenting the 3,5-diarylisoxazole embedded in a single molecular plane (σ) the excluded volume for series **9** tends to increase upon heating and, consequently, the void volume between molecules becomes progressively high against anisotropic interaction of the mesogens. These intermolecular forces are not enough to sustain molecules close together in the mesophase for a long period of time as the temperature increases. Molecules of series **9** in the isotropic state rotate and translate freely in the available space than in the mesophase. In the LC state for series **9**, molecules are hindered to rotate or translate and, therefore, molecule motions are greatly hindered and the LC state has low rotational and translational entropy. When going to the isotropic state, molecules gain considerable rotational and translational entropy and the transition from mesophase to liquid state to series **9** is driven mostly by entropic effect. Before reach the isotropic state, molecules for series **9** undergo to thermal expansion in direction of short aryl group represented by blue bowl in Figure 8. The expansion induced by the heat is responsible in some extension for the predominance of SmA mesophase for series **9**. For series **10**, molecules are not greatly hindered due to planarization and conjugation of the heterocyclic ring. The void volume is reduced with gains in anisotropic (attractive forces) interactions, and the balance between the minimization of free volume and attractive forces manifests itself through a large mesophase range and, consequently, low enthalpy and entropy values at the transition from the mesophase to the isotropic state (Figure 8).

In the mesophase, linearity, flatness, and conjugation contribute significantly to the molecules slides one over the others easier for a large superficial area. The orientational order in this circumstance is maintained through the anisotropic interactions (π-stacking) due to higher molecular anisometry. However, those attributes vanish and molecular fold overlaps and orientational or translational motion become more diffuse because of the loss of anisotropic interactions. The entanglement of the alkylaryl chains (blue ball and stick in Figure 8) of the non-linear molecules (**9**) distributed in two molecular planes also contributes

decisively to the shortening of the observed mesophase range and, consequently, to the reduction in the clearing temperature. The entanglements of the two distinct aryl groups at the 3- and 5-position of the isoxazoline ring located in the main plane (σ) and a secondary plane (σ´) inhibit the rotational and translational diffusion in the mesophase. Figure 8c briefly describes the molecular packing for series **9**, where we are assuming that the sliding of the layers is reached only when the free space for every molecule is available. Piles of molecules in racemic or homoquiral domains will be able to flow freely in the liquid state only when individual molecules overcome the volume defined by the alkylaryl groups of the σ´ plane, with an increase in the corresponding entropy due to the thermal expansion (Table 1 and Table 2). Also, the chiral carbon atom in **9c10** contributes to the enthalpy value since every single chiral carbon atom on every single isoxazoline molecule presents residual polarization, and neutrality comes from the other isomer with opposite handness (Figure 8d).[52] Compounds of series **9**, considering the void volume, behave similar to side-chain polymers with bulky side groups presenting high glass transitions.[53]. The void volume for isoxazolines is bigger than isoxazoles due to the interwoven continuos and alternates networks (Figure 8). Due to the intertwining of the molecular planes, the liquid state is reached only after all the intermolecular interactions between the planes have broken down. To be able to flow freely, molecules of series **9** must initially expand laterally across the secundary sigma plane with increasing void volume. Lateral diffusion come first and then the molecules can slide one molecule over the other logitudinally.In this way, the mesophases and thermal data of series **9** and **10** can be understood according to Figure 9. The enthalpic factor is the main driving force for maintaining close together molecules for series **10**, while entropy is determinant factor for molecules of series **9**. For any fluid phase transition, these two molecular planes carrying aromatic groups are sterically hindered to flow freely in the mesophase. X-ray data reveals that in a wide angle region the intermolecular distance for **9c10** is higher than for **10c10**, which is consistent with the formation of racemic or homoquiral domains.

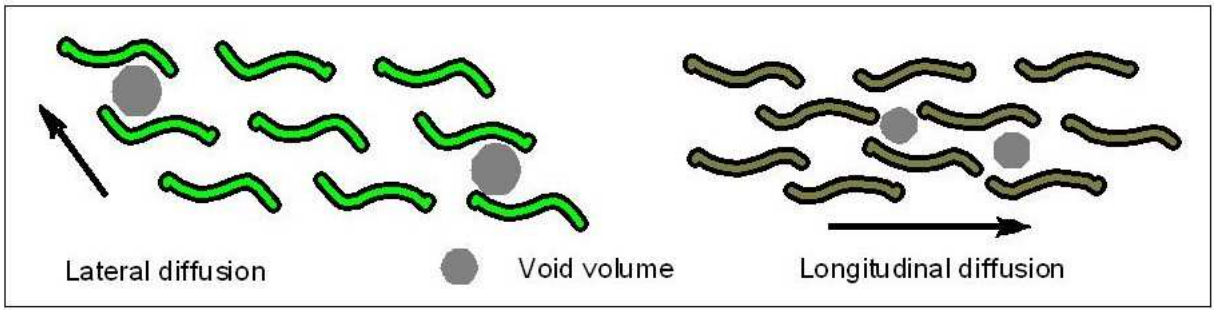

Figure 9. Schematic model of the clearing process. Black arrows give the lateral and longitudinal diffusion for **9** and **10** series, respectively. Gray circles represent the free space generated by translation of the non-linear molecules. For clarification (simplification), the molecular fold for **9** is not seen by the blue ball, as shown in Figure 8.

In the melting process, the solid crystal collapses due to the increase in molecular fluctuation, vibration, and rotation of atoms through chemical bonds. The energy of the crystal lattice that evolved at the transition is partially retained in the mesophase. Steric considerations of the solid state are critical for non-linear molecules where the void volume tends to increase as the molecular bend changes from the σ plane to σ´ plane. Molecular packing and electrostatic interactions in the solid-state are adjusted in such a way that they determine the melting temperature of the solid. Of course, if the heat used to melt the material is too high, the dynamic process between anisotropic attractive forces and packing issues to sustain the long-range orientational order is lost and no mesophase will be formed. Thus, the geometry and packing considerations are closely related with the mesophase nature and transition temperature. Data in Table 1 and Table 2 establish a puzzling game, where more anisometric mesogens for series **10** present a larger mesophase range than series **9**, with a predominance of the nematic mesophase and higher enthalpy and entropy values for the melting process and lower values for the transition between the mesophase and the isotropic state. Conversely, the less anisometric series **9** displays in general lower values for the transition from the crystal state to the mesophase and higher values for the mesophase to the isotropic state. The precise adjustment of electrostatic and packing preferences favours the propagation of a long-range orientational order in more anisometric molecules such as series **10**, while positional order or lateral diffusion by thermal expansion favours the less linear molecules of series **9**, favoured due to residual polarization of the chiral centre by molecular bending of SBs containing the isoxazoline ring. As pointed out by Pinal[54], melting temperature is dependent on the molecular symmetry (Carnelley´s rule). Data in Table 1 and Table 2 related to the melting point for SBs of series **9** and **10** display, in general, divergent behaviour of the Carnelley´s rule. Most compounds that belong to series **9** present melting temperatures higher than compounds of series **10**, which is probably an exception to this rule. As an example, consider **9bn/9cn** and **10bn/10cn** SBs, where this violation is clearly seen for less symmetric compounds having higher melting points. In addition, an interesting effect is seen for **9bn/9cn** compounds containing an alkyl chain and halogen atoms as terminal groups. The melting point decreases as the alkyl chain increases, and **9bn/9cn** present almost the same clearing transition temperature around 184°C, which highlights the entropic effect that the alkyl chains have on the crystal phase for isoxazolines rather than isoxazoles.

X-ray diffraction measurements, as shown in Figure 10, were carried out with the selected **9c10** and **10c10** compounds to confirm the lamellar structure and to obtain the interlayer spacing of the SmA mesophase. For both compounds, the d_{001}/d_{002} ratio is approximately equal to 2, which is consistent with a molecular lamellar structure. The interlayer spacings of 34.0 Å and 36.3 Å for compounds **9c10** and **10c10**, respectively, are a little longer than their calculated molecular lengths (31.8 Å and 32.5 Å), considering the most extended configuration. Bent-shaped molecules can present an out-of-layer fluctuation (OLF) at the interfacial curvature, independent of whether molecules assume synclinic or anticlinic configurations.[50] Therefore, increasing the interlayer spacing as a result of this kind of fluctuation is common to smectic liquid crystals.

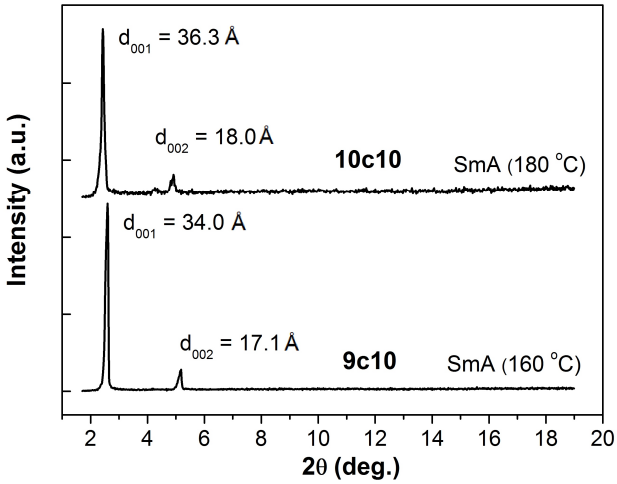

Figure 10. X-ray diffractogram of compounds **9c10** and **10c10** captured at 160°C and 180°C, respectively. The **9c10** spectrum was divided by a factor of 3 and **10c10** vertically translated for better view.

3. Conclusions

In summary, liquid-crystalline SBs containing 5-membered isoxazoline **9** and isoxazole **10** were evaluated using DSC, POM, X-ray, and DFT calculations. A puzzling game was established related to the mesomorphic properties by comparison of the enthalpy and entropy data. They were used to justify the intricate thermal behaviour for both series, transition temperatures between the crystal phase to the mesophase and the mesophase to the liquid phase. The mesophase range and the nature of the mesophase were analysed based on packing issues and anisotropic interactions. The void volume was tentatively assigned as one of the major causes of this complicated behaviour, especially for compounds of the SBs **9**. In general, enthalpy and entropy values were considerably high for more anisometric SBs belonging to series **10** in the transition from the crystal phase to the mesophase, while those energetic values were inverted, favouring the less anisometric SBs belonging to series **9** in the transition from the mesophase to the isotropic phase. Melting points were higher for series **9** than series **10** and clearing temperatures displayed the opposite behaviour. From the thermal data, we have concluded that the entropy effect acts in favour of series **9**, while enthalpy is the driving force for series **10**. The relationship between structure and liquid crystals properties was also supported by X-ray diffraction data by indexation of Miller peaks for two SBs (**9c10** and **10c10**) and through DFT calculations. Molecular folding (bending) of the main molecular axis was determinant in the nature and stabilization of the mesophase. SBs **10** have an in-plane bent-core shape and displayed a huge mesophase range with a predominance of the N mesophase. On the other hand, SBs **9** are out-of-plane bent-core shape and showed a small mesophase range with a predominance of the smectic mesophase.

Conflicts of interest

There are no conflicts to declare.

Acknowledgements

This work was supported by the CNPq/Edital Universal [n° 011/2016/403075/2016-5 and 407773/2016-9], CAPES, and INCT-INEO. This study was financed in part by the Coordenação de Aperfeiçoamento de Pessoal de Nível Superior, Brasil (CAPES) [Finance Code 001].

Notes and references

[1]. J. Kim, H. Kim, and S. B. Park, *J. Am. Chem. Soc.*, 2014, **136**, 14629. https://doi.org/10.1021/ja508343a

[2]. G. N. Pairas, F. Perperopoulou, P. G. Tsoungas and G. Varvounis, *ChemMedChem*, 2017, **12**, 408. https://doi: 10.1002/cmdc.201700023

[3]. A. P. Kozikowski, *Acc. Chem. Res.*, 1984, **17**, 410. https://doi.org/10.1021/ar00108a001

[4]. K. Kaur, V. Kumar, A. K. Sharma, G. K. Gupta. *European Journal of Medicinal Chemistry*, 2014, **77**, 121. https://doi: 10.1016/j.ejmech.2014.02.063

[5]. N. Agrawal and P. Mishra. *Medicinal Chemistry Research*, 2018, **27**, 1309. https://doi.org/10.1007/s00044-018-2152-6

[6]. T. Weber and P. M. Selzer, Edited by S. Müller, R. Cerdan and O. Radulescu, 2016 Wiley-VCH Verlag GmbH & Co. KGaA, Weinheim, Germany.

[7]. S. Tilvi and K. S. Singh. *Current Organic Chemistry*, 2016, **20**, 898. https://doi: 10.2174/1385272819666150804000046

[8]. A. Kulyashova and M. Krasavin, *Tetrahedron Letters*, 2016, **57**, 4395. https://doi.org/10.1016/j.tetlet.2016.08.059

[9]. S. Stosic-Grujicic, I. Cvetkovic, K. Mangano, M. Fresta, D. Maksimovic-Ivanic, L. Harhaji, D. Popadic, M. Momcilovic, D. Miljkovic, J. Kim, Y. Al-Abed and F. Nicoletti, *J. Pharm. Exp. Therapeutics*, 2007, **320**, 1038. https://doi: 10.1124/jpet.106.109272

[10]. G. Shakya, H. Rivera Jr, D. J. Lee, M. J. Jaremko, J. J. La Clair, D. T. Fox, R. W. Haushalter, A. J. Schaub, J. Bruegger, J. F. Barajas, A. R. White, P. Kaur, E. R. Gwozdziowski, F. Wong, S. Tsai, M. D. Burkart. *J. Am. Chem. Soc.*, 2014, **136**, 16792. https://doi.org/10.1021/ja5064857

[11]. R. Orth, T. Böttcher and S. A. Sieber, *Chem. Commun.*, 2010, **46**, 8475. https://doi: 10.1039/C0CC02825H

[12]. J. J. Talley, D. L. Brown, J. S. Carter, M. J. Graneto, C. M. Koboldt, J. L. Masferrer, W. E. Perkins, R. S. Rogers, A. F. Shaffer, Y. Y. Zhang, B. S. Zweifel and K. Seibert, *J. Med. Chem.*, 2000, **43**, 775. https://doi.org/10.1021/jm990577v

[13]. A. Kamal, A. Viswanath, M. Janaki Ramaiah, J. N. S. R. C. Murty, F. Sultana, G. Ramakrishna, J. R. Tamboli, S. N. C. V. L. Pushpavalli, D. Pal, C. Kishor, A. Addlagatta and M. pal Bhadra, *Med. Chem. Commun.*, 2012, **3**, 1386. https://doi: 10.1039/C2MD20085F

[14]. J. Cao and X. Huang, *J. Comb. Chem.*, 2008, **10**, 526. https://doi.org/10.1021/cc800034v

[15]. N. A. Zafiropoulos, E. Choi, T. Dingemans, W. Lin and E. T. Samulski, *Chem. Mater.*, 2008, **20**, 3821. https://doi.org/10.1021/cm701862w

[16]. J. W. Goodby, R. J. Mandle, E. J. Davis, T. Zhong and S. J. Cowling, *Liquid Crystals*, 2015, **42**, 593. https://doi: 10.1080/02678292.2015.1030348

[17]. W. Weissflog, U. Baumeister, M. Tamba, G. Pelzl, H. Kresse, R. Friedemann, G. Hempel, R. Kurz, M. Roos, K. Merzweiler, A. Jákli, C. Zhang, N. Diorio, R. Stannarius and A. E. U. Kornek, *Soft Matter*, 2012, **8**, 2671. https://doi 10.1039/C2SM07064B

[18]. M. Alaasar, S. Poppe, C. Tschierske, *Journal of Molecular Liquids*, 2019, **277**, 233. https://doi.org/10.1016/j.molliq.2018.12.088

[19]. S. Maisch, A. Krause, D. Schmidt and M. Lehmann, *Liquid Crystals*, 2018, **45**, 136. https://doi.org/10.1080/02678292.2017.1369595

[20]. E. J. Foster, R. B. Jones, C. Lavigueur and V. E. Williams, *J. Am. Chem. Soc.*, 2006, **128**, 8569. https://doi.org/10.1021/ja0613198

[21]. T. Zhong, R. J. Mandle, I. Saez, S. Cowling and J. W. Goodby, *Liquid Crystals*, 2018, **45**, 2274. https://doi: 10.1080/02678292.2018.1515371

[22]. S. Laschat, A. Baro, N. Steinke, F. Giesselmann, C. Hägele, G. Scalia, R. Judele, E. Kapatsina, S. Sauer, A. Schreivogel and M. Tosoni, *Angew. Chem. Int. Ed.*, 2007, **46**, 4832. https://doi: 10.1002/anie.200604203.

[23]. S. Kang, Y. Saito, N. Watanabe, M. Tokita, Y. Takanishi, H. Takezoe and J. Watanabe, *J. Phys. Chem. B*, 2006, **110**, 5205. https://doi.org/10.1021/jp057307a

[24]. D. Demus, *Liquid Crystals*, 1989, **5**, 75. https://doi.org/10.1080/02678298908026353

[25]. J. P. F. Lagerwall, F. Giesselmann, M. D. Wand and D. M. Walba, *Chem. Mater.*, 2004, **16**, 3606. https://doi.org/10.1021/cm035294c

[26]. O. M. S. Ritter, F. C. Giacomelli, J. A. Passo, N. P. da Silveira and A. A. Merlo, *Polymer Bulletin*, 2006, **56**, 549. https://doi: 10.1007/s00289-006-0526-2

[27]. A. Tavares, J. M. Toldo, G. D. Vilela, P. F. B. Gonçalves, I. H. Bechtold, S. P. Kitney, S. M. Kelly and A. A. Merlo, *New J. Chem.*, 2016, **40**, 393. https://doi: 10.1039/C5NJ02199E

[28]. V. Bezborodov, N. Kauhanka and V. Lapanik, *Mol. Cryst. Liq. Cryst.*, 2004, **411**, 1145. https://doi.org/10.1080/15421400490434874

[29]. H. Gallardo, C. Zucco and L. da Silva, *Mol. Cryst. and Liq. Cryst.*, 2002, **373**, 181. https://doi.org/10.1080/10587250210533

[30]. U. M. Kauhanka and M. M. Kauhanka, *Liquid Crystals*, 2006, **33**, 121. https://doi.org/10.1080/02678290500429976

[31]. H. Kuo, S. Tsai, G. Lee, H. Sheu and C. K. Lai, *Tetrahedron*, 2013, **69**, 618. https://doi.org/10.1016/j.tet.2012.11.013

[32]. T. Haino, M. Tanaka, K. Ideta, K. Kubo, A. Mori and Y. Fukazawa, *Tetrahedron Letters*, 2004, **45**, 2277. https://doi.org/10.1016/j.tetlet.2004.01.116

[33]. V. N. Kovganko and N. N. Kovganko, *Russian Journal of Organic Chemistry*, 2006, **42**, 430. https://doi 10.1134/S1070428006060169

[34]. J. Barbera, R. Gimenez, J. L. Serrano, R. Alcala, B. Villacampa, J. Villalba, I. Ledoux and J. Zyss, *Liquid Crystals*, 1997, **22**, 265. https://doi.org/10.1080/026782997209315

[35]. A. Tavares, P. R. Livotto, P. F. B. Gonçalves and A. A. Merlo, *J. Braz. Chem. Soc.*, 2009, **20**, 1742. http://dx.doi.org/10.1590/S0103-50532009000900025

[36]. R. R. da Rosa, Isoxazolinas e Isoxazóis como reais candidatos na preparação de cristais líquidos polares. PhD Thesis, 2018, Instituto de Química, UFRGS, Brazil. http://hdl.handle.net/10183/180639.

[37]. A. Tavares, M. Tariq, S. Hameed, I. H. Bechtold, P. R. Livotto, and A. A. Merlo, 26th International Liquid Crystal Conference (ILCC2016-346). 2016, Kent, Ohio, USA.

[38]. J. M. F. M. Schneider, E. S. Sales, P. R. Livotto, Paulo H. Schneider and A. A. Merlo, *J. Braz.Chem. Soc.*, 2014, **25**, 1493. http://dx.doi.org/10.5935/0103-5053.20140132

[39]. L. Fritsch and A. A. Merlo, *ChemistrySelect*, 2016, **1**, 23. https://doi.org/10.1002/slct.201500044

[40]. L. Fritsch, V. L. Lavayen and A. A. Merlo, *Liquid Crystals*, 2018, **45**, 1802. https://doi.org/10.1080/02678292.2018.1488280.

[41]. G. D. Vilela, R. R. da Rosa, P. H. Schneider, I. H. Bechtold, J. Eccher and A. A. Merlo, *Tetrahedron Lett.*, 2011, **52**, 6569. https://doi.org/10.1016/j.tetlet.2011.09.122

[42]. L. J. Kately, W. B. Martin, D. C. Wiser and C. A. Brummond, *J. Chem. Educ.*, 2002, **79**, 225. https://doi.org/10.1021/ed079p225

[43]. N. A. Clark and R. B. Meyer, *Appl. Phys. Lett.*, 1973, **22**, 493. https://doi.org/10.1063/1.1654481

[44]. B. I. Senyuk, I. I. Smalyukh and O. D. Lavrentovich, *Physical Review E*, 2006, **74**, 011712. https://doi.org/10.1103/PhysRevE.74.011712

[45]. I. Dierking, Texture of liquids crystals, Wiley VHC, Revised edition, 2003.

[46]. M. J. Frisch, G. W. Trucks, H. B. Schlegel, G. E. Scuseria, M. A. Robb, J. R. Cheeseman, G. Scalmani, V. Barone, B. Mennucci, G. A. Petersson, H. Nakatsuji, M. Caricato, X. Li, H. P. Hratchian, A. F. Izmaylov, J. Bloino, G. Zheng, J. L. Sonnenberg, M. Hada, M. Ehara, K. Toyota, R. Fukuda, J. Hasegawa, M. Ishida, T. Nakajima, Y. Honda, O. Kitao, H. Nakai, T. Vreven, J. A. Montgomery Jr., J. E. Peralta, F. Ogliaro, M. J. Bearpark, J. Heyd, E. N. Brothers, K. N. Kudin, V. N. Staroverov, R. Kobayashi, J. Normand, K. Raghavachari, A. P. Rendell, J. C. Burant, S. S. Iyengar, J. Tomasi, M. Cossi, N. Rega, N. J. Millam, M. Klene, J. E. Knox, J. B. Cross, V. Bakken, C. Adamo, J. Jaramillo, R. Gomperts, R. E. Stratmann, O. Yazyev, A.J. Austin, R. Cammi, C. Pomelli, J.W. Ochterski, R. L. Martin, K. Morokuma, V. G. Zakrzewski, G. A. Voth, P. Salvador, J. J. Dannenberg, S. Dapprich, A. D. Daniels, Ö. Farkas, J. B. Foresman, J. V. Ortiz, J. Cioslowski, D. J. Fox, Gaussian 09 Rev. D01, Gaussian, Inc., Wallingford, CT, USA, 2009.

[47]. L. D. Lopes, A. J. Bortoluzzi, G. Prampolini, F. P. Santos, P. R. Livotto and A. A. Merlo, *J. Fluorine Chemistry*, 2018, **211**, 24. https://doi.org/10.1016/j.jfluchem.2018.04.007

[48]. M. M. Lobo, C. M. Viau, J. M. dos Santos, H. G. Bonacorso, M. A. P. Martins, S. S. Amaral, J. Saffi and N. Zanatta, *European Journal of Medicinal Chemistry*, 2015, **101**, 836. https://doi.org/10.1016/j.ejmech.2015.06.040

[49]. O. B. Bondarenko, A. Y. Gavrilova, V. V. Polunina, Z. A. Starikova, N. V. Zyk, N. S. Zefirov, *Mendeleev Communications*, 2009, **19**, 12. https://doi.org/10.1016/j.mencom.2009.01.005

[50]. M. A. Glasser and N. A. Clark, *Physical Review E*, 2002, **66**, 021711. https://doi.org/10.1103/PhysRevE.66.021711

[51]. N. Hu, R. Shao, C. Zhu, Y. Shen, C. Park, E. Korblova, C. Guerra, J. A. Rego, A. Hexemer, N. A. Clark and D. M. Walba, *Chemical Science*, 2014, **5**, 1869. https://doi.org/10.1039/C3SC53353K

[52]. Alan Berthod, *Anal. Chem.*, 2006, **78**, 2093. https://doi.org/10.1021/ac0693823

[53]. M. Portugall, H. Ringsdorf, R. Zentel. *Makromol. Chem*,. 1982, **183**, 2311https://doi.org: 10.1002/macp.1982.021831003

[54]. R. Pinal, *Org. Biomol. Chem.*, 2004, **2**, 2692. https://doi.org/10.1039/B407105K

Highlights

- Synthesis of Schiff bases (SBs) containing isoxazoline and isoxazole rings.
- Entropy and enthalpy effects dictated the liquid crystals properties.
- Molecular geometry of heterocyclic is critical on mesomorphic behaviour.
- Isoxazoline SBs were predominantly smectics while isoxazoles SBs were nematics.
- Lateral and longitudinal diffusion were express in terms of molecular geometry.

Conflicts of interest

No potential conflict of interest was reported by the authors.